processes

MDPI

Article

Effect of the Marangoni Convection in the Unsteady Thin Film Spray of CNT Nanofluids

Ali Rehman [1], Taza Gul [2], Zabidin Salleh [1], Safyan Mukhtar [3], Fawad Hussain [4], Kottakkaran Sooppy Nisar [5] and Poom Kumam [6,7,8,*]

1 School of Informatic and Applied Mathematics, University Malaysia Terengganu, Kuala Nerus 21030, Terengganu, Malaysia; alirehmanchd8@gmail.com (A.R.); zabidin@umt.edu.my (Z.S.)
2 Department of mathematics, City University of Science and Information Technology, Peshawar 25000, Pakistan; tazagul@cusit.edu.pk
3 Preparatory Year Deanship, King Faisal University, Hofuf 31982, Al-Hasa, Saudi Arabia; smahmad@kfu.edu.sa
4 Department of Mathematics, Abbottabad University of Science and Technology Abbottabad 22010, Pakistan; fawad.hussain30@gmail.com
5 Department of Mathematics, College of Arts and Sciences, Wadi Aldawaser, Prince Sattam bin Abdulaziz University, Al-Kharj 11991, Saudi Arabia; n.sooppy@psau.edu.sa
6 KMUTT-Fixed Point Research Laboratory, Room SCL 802 Fixed Point Laboratory, Science Laboratory Building, Department of Mathematics, Faculty of Science, King Mongkut's University of Technology Thonburi (KMUTT), 126 Pracha-Uthit Road, Bang Mod, Thrung Khru, Bangkok 10140, Thailand
7 KMUTT-Fixed Point Theory and Applications Research Group, Theoretical and Computational Science Center (TaCS), Science Laboratory Building, Faculty of Science, King Mongkut's University of Technology Thonburi (KMUTT), 126 Pracha-Uthit Road, Bang Mod, Thrung Khru, Bangkok 10140, Thailand
8 Department of Medical Research, China Medical University Hospital, China Medical University, Taichung 40402, Taiwan
* Correspondence: poom.kum@kmutt.ac.th

Received: 3 April 2019; Accepted: 3 June 2019; Published: 24 June 2019

Abstract: The gradient of surface temperature is known as Marangoni convection and plays an important role in silicon melt, spray, atomic reactors, and thin fluid films. Marangoni convection has been considered in the liquid film spray of carbon nanotube (CNT) nanofluid over the unsteady extending surface of a cylinder. The two kinds of CNTs, single-wall carbon nanotubes (SWCNTs) and multiple-wall carbon nanotubes (MWCNTs), formulated as water-based nanofluids have been used for thermal spray analysis. The thickness of the nanofluid film was kept variable for a stable spray rate and pressure distribution. The transformed equations of the flow problem have been solved using the optimal homotopy analysis method (OHAM). The obtained results have been validated through the sum of the total residual errors numerically and graphically for both types of nanofluids. The impact of the physical parameters versus velocity, pressure, and temperature pitches under the influence of the Marangoni convection have been obtained and discussed. The obtained results are validated using the comparison of OHAM and the (ND-solve) method.

Keywords: Marangoni convection; SWCNT/MWCNT nanofluid; extending cylinder; OHAM and ND-solve methods

1. Introduction

The discrepancy which occurs due to the two surface tensions of two fluids, or between the plate surface and fluid, formed by the temperature gradient is known as thermal Marangoni convection. The surface temperature gradient generates the Marangoni stream and plays an important role in silicon melt, precious stone development, ignition, spray and coating, atomic reactors, and thin fluid

films. Chen [1] experimented with liquid film using the power law model with Marangoni convection over an unstretched sheet. He observed the impact of the physical parameters under the influence of Marangoni convection. The interface study has wide applications in the fields of engineering [2,3], energy, and fuels [4,5]. These interfaces are usually used for the separation of materials, layers, and so on.

Nanofluid is defined as the homogeneous mixture of nanosized particles and base fluids. Basically, the thermal conductivity of conventional base liquids, such as oil, ethylene, water, etc., is comparatively low. Therefore, nanosized (1–100 nm) metal particles are mixed in the base fluid at up to 50% of the base fluid. This enhances the thermal conductivity and heat transfer rate significantly. Kumar et al. [6] examined nanofluid flow in the existence of a heat source/sink under the Marangoni convection effect.

The carbon nanotube (CNT) is the most popular class of the carbon family for the enhancement of heat transfer devices. This class is further divided into subclasses, known as single- and multiple-wall carbon nanotubes (SWCNTs/MWCNTs). CNTs are widely used in engineering applications such as fluidization reactors and the heat exchange cooling industry. Haq et al. [7] have investigated nanofluid thermal management over a trapezoidal cavity under Marangoni convection. They observed the impact of the physical constraints under Marangoni convection and found that the temperature is enhanced with the partially heated domain. In 1991, Lijima discovered carbon nanotubes (CNTs) and inspected multiple-wall carbon nanotubes (MWCNTs) for the first time using the Krastschmer and Huddman technique [8]. Later on, in 1993, Donald Bethune inspected single-wall carbon nanotubes (SWCNTs) [9]. SWCNTs are a rolled sheet of graphene in a tube or cylinder shape with a diameter range of 0.4×10^{-9} m to 3×10^{-9} m and a thickness of about 0.34×10^{-9} m [10], whereas MWCNTs consist of 2 to 50 coaxial nanotubes with 0.34×10^{-9} m layer spacing and diameter ranging from 3×10^{-9} m to 30×10^{-9} m [11]. Hone [12] identified that thermal conductivity is achieved up to 6600 $Wm^{-1}K^{-1}$ for SWCNTs and 3000 $Wm^{-1}K^{-1}$ for MWCNTs at room temperature. Haq et al. [13] showed that engine oil-based CNTs have a greater value of skin friction as well as heat transfer rate than simple water- and kerosene oil-based CNTs. Khan et al. [14] discussed the thermal conductivity and Navier slip boundary condition for the flow of both CNTs along a plate. Kamli et al. [15] studied the models of the power law and convective heat analysis using CNT-based nanofluid with constant heat flux. Lie et al. [16] examined CNTs in the presence of engine oil and ethylene glycol as ordinary liquids. They showed that the thermal efficiency of CNTs in engine oil-based nanofluid is higher than that without CNTs, and a similar result was obtained in the case of ethylene glycol. At a volume fraction of 0.02, the thermal efficiency of engine oil was increased by 30%, while this was increased by 12.4% in the CNT ethylene glycol-based nanofluid with a volume fraction of 0.01. In another study, the efficiency of coolant water-based nanofluid CNTs was reported by Halelfadel et al. [17].

Some researchers [18–20] have used various thermal conductivity models for a range of mathematical problems. All of the thermal conductivity models have important applications related to the nature of nanofluids. Xue [21] introduced the thermal conductivity model for CNT nanofluids. This thermal conductivity model is frequently used for CNT nanofluids [22–24].

The heat and mass transfer within a liquid is an interesting area of research; as liquid film flow is used in coating industries as a fiber coating and wire coating, it is a requirement of every coating process that the rate of coating and mass transfer within the liquid is ideal. The boundary layer is usually considered in the infinite domain, while the liquid film is in the finite and small domain. Wang [25] is the pioneer in the investigation of liquid film flow over a stretched sheet in its unsteady form. Later on, this idea was further developed by researchers such as Anderson et al. [26], Chen [27,28], Wang [29], Dandapat et al. [30], Liu and Anderson [31,32], Abel et al. [33], and Nandeppanavar [34].

The thin film spray over an extending cylinder with slip and no-slip conditions using a variety of viscous fluids and nanofluids was examined by Wang [35], Khan et al. [36], Shomrani and Gul [37], and Gul et al. [38].

In all of the existing literature, the spray phenomenon has been investigated under the effect of physical parameters. The present study focuses on the thin film spray under the impact of Marangoni convection. SWCNT/MWCNT water-based nanofluids are used for the thermal spray analysis. A discrepancy in the effect of the physical parameters is observed due to the influence of Marangoni convection. The solution to the problem is obtained using the optimal homotopy analysis method (OHAM) [39]. The stability of the problem is also obtained up to the 30th-order approximation using the BVPh 2.0 package [40–42]. The outputs are displayed and discussed.

2. Mathematical Formulation

The thin film spray was considered over a stretching cylinder. Nanoparticles of the two types of CNTs, named SWCNTs and MWCNTs, were suspended in water to create the nanofluids. The thickness of the thin film is considered to be δ. The surface of the cylinder is stretchable along the z axis and the stretching velocity is $W_w = 2cz$.

The radius of the cylinder is a, and b is the radius of the thickness of the thin film above the cylinder surface. All other assumptions are selected as detailed elsewhere [24–27].

The basic flow equations are as follows:

$$\frac{\partial u}{\partial r} + \frac{u}{r} + \frac{\partial w}{\partial z} = 0, \tag{1}$$

$$\rho_{nf}\left(u\frac{\partial u}{\partial r} + w\frac{\partial u}{\partial z}\right) = -\frac{\partial p}{\partial r} + \mu_{nf}\left(\frac{1}{r}\frac{\partial u}{\partial r} - \frac{u}{r^2} + \frac{\partial^2 u}{\partial r^2}\right), \tag{2}$$

$$\rho_{nf}\left(u\frac{\partial w}{\partial r} + w\frac{\partial w}{\partial z}\right) = \mu_{nf}\left(\frac{1}{r}\frac{\partial w}{\partial r} + \frac{\partial^2 w}{\partial r^2}\right), \tag{3}$$

$$\rho_{nf}\left(u\frac{\partial T}{\partial r} + w\frac{\partial T}{\partial z}\right) = \frac{k}{(\rho C_p)_{nf}}\left(\frac{1}{r}\frac{\partial T}{\partial r} + \frac{\partial^2 T}{\partial r^2}\right), \tag{4}$$

Here, $w(r,z)$ is the velocity along the $z-axis$ and $u(r,z)$ is the velocity along the radial axis. ρ_{nf} is the density of the nanofluid, μ_{nf} is the viscosity of the nanofluid, p is the is the thermal conductivity of the nanofluid, and $(C_p)_{nf}$ is the heat capacitance of the nanofluid. The appropriate boundary conditions under the Marangoni convection are as follows:

$$u = U_w,\ w = W_w,\ T = T_w \ \ at \ \ r = a, \tag{5}$$

$$\mu_{nf}\frac{\partial w}{\partial r} = \left(\frac{\partial \sigma^{\otimes}}{\partial T}\right)\frac{\partial T}{\partial z},\ \ u = w\left(\frac{\mathrm{d}\,\delta}{\mathrm{d}\,z}\right),\ \ \frac{\partial T}{\partial \mathrm{r}} = 0 \ \ at \ \ r = b. \tag{6}$$

Here, $\sigma^{\otimes} = \sigma_0[1 - \gamma(T - T_b)]$ is the surface tension and $\gamma = \left(\frac{\partial \sigma^{\otimes}}{\partial T}\right)_{T=T_0}$ and σ_0 are the positive constants. $U_w = -ca$ is the suction and injection velocity, depending on the positive and negative values of c. The wall temperature is defined as

$$T_w(z) = T_b - T_{ref}\left(\frac{cz^2}{\upsilon}\right), \tag{7}$$

The temperature at the external surface of the liquid film is denoted by T_b, and T_{ref} is the reference temperature such that $0 \le T_{ref} \le T_b$.

The similarity variables satisfy the necessary conditions [36–38] and are displayed as follows:

$$u = -ca\frac{f(\eta)}{\sqrt{\eta}},\ w = 2cz\frac{df}{d\eta},\ T = T_b - T_{ref}\left(\frac{cz^2}{\upsilon}\right)\theta(\eta),\ \text{where}\ \eta = \left(\frac{r}{a}\right)^2 \tag{8}$$

$$\eta = \left(\frac{b}{a}\right)^2 = \beta. \tag{9}$$

Here, β is the dimensionless thickness of the liquid film and b is the exterior radius of the liquid film. The thermophysical constraints for the nanofluids are as follows:

$$\begin{aligned} &\frac{\rho_{nf}}{\rho_f} = (1-\phi) + \phi\left(\frac{\rho_{CNT}}{\rho_f}\right),\ \frac{\mu_{nf}}{\mu_f} = (1-\phi)^{-2.5}, \frac{(\rho\ Cp)_{nf}}{(\rho\ Cp)_f} = \left[(1-\phi) + \phi\left(\frac{(\rho\ cp)_{CNT}}{(\rho\ cp)_f}\right)\right], \\ &\frac{k_{nf}}{k_f} = \frac{1-\phi+2\phi\left(\frac{k_{CNT}}{k_{CNT}-k_f}\right) ln\left(\frac{k_{CNT}+k_f}{2\,k_f}\right)}{1-\phi+2\phi\left(\frac{k_f}{k_{CNT}-k_f}\right) ln\left(\frac{k_{CNT}+k_f}{2\,k_f}\right)}. \end{aligned} \tag{10}$$

In the above expression, ϕ is the nanoparticle volume fraction and ρ_f, $\left(\rho\ C_p\right)_f$, ρ_{CNT}, $\left(\rho\ C_p\right)_{CNT}$ are the density and specific heat capacities of the base fluid and CNTs, respectively.

Thermophysical properties of the base solvent water and solid materials of CNT nanoparticles are specified in Table 1.

Table 1. The thermophysical properties of single- and multiple-wall carbon nanotubes (SWCNTs/ MWCNTs) and the base fluid (water).

Model		$\boldsymbol{\rho}$ **(kg/m^3)**	$\boldsymbol{Cp}$ **(J/kg K)**	$\boldsymbol{K}$ **(W/mk)**
Water (W)		997.1	4179	0.613
Nanoparticles	SWCNT	2600	425	6600
	MWCNT	1600	796	3000

The similarity variables in Equation (8) are inserted into Equations (1)–(6), and the dimensionless equations are obtained as follows:

$$(\eta f''' + f'') - \mathrm{Re}(1-\phi)^{2.5}\left(1-\phi+\phi\frac{\rho_{CNT}}{\rho_f}\right)\left[(f')^2 - ff''\right] = 0, \tag{11}$$

$$\frac{k_{nf}}{k_f}(\eta\theta'' + \theta') - \mathrm{RePr}\left((1-\phi) + \phi\frac{(\rho C_p)_{CNT}}{(\rho C_p)_f}\right)[2f'\theta - f\theta' 2f'\theta - f\theta'] = 0, \tag{12}$$

$$f(\eta) = 0,\ f''(\eta) = (1-\phi)^{2.5}\frac{M}{\sqrt{\eta}}\theta(\eta),\ \ \theta'(\eta) = 0 \text{ at } \eta = \beta. \tag{13}$$

Here, f, θ, and β are the dimensionless forms of velocity, temperature, and film thickness. The physical parameters obtained from the transformation are:

$$\mathrm{Re} = \frac{ca^2}{2\upsilon_f}, \mathrm{Pr} = \frac{(\mu C_p)_f}{k_f}, M = \frac{a\gamma\delta_0 T_{ref}}{\upsilon_f}. \tag{14}$$

Here, M, Pr and Re are the Marangoni constraint, Prandtl number and Reynolds number. The similarity variables in Equation (8) are utilized in Equation (3) to obtain the pressure term as follows:

$$\frac{P-P_\infty}{c\mu_f} = -\frac{\mathrm{Re}f^2}{\eta}(1-\phi)^{2.5}\left(1-\phi+\phi\frac{\rho_{CNT}}{\rho_f}\right) - 2f'. \tag{15}$$

The transformed shear stress on the film exterior portion is

$$f''(\beta) = M\,\theta(\beta)\,(1-\phi)^{2.5}. \tag{16}$$

The shear stress on the wall is

$$\tau = \frac{4c\mu z}{a} f''(1). \tag{17}$$

The deposition velocity V is defined as

$$-\mathrm{V} = -ca\frac{f(\beta)}{\sqrt{\beta}}, \tag{18}$$

The mass flux m_1 per axial length is expressed as

$$m_1 = 2\pi b\mathrm{V} \tag{19}$$

The normalized mass flux m_2 is

$$m_2 = \frac{m_1}{2\pi a^2 c} = \frac{m_1}{4\pi \upsilon \mathrm{Re}} = f(\beta) \tag{20}$$

The local Skin friction and Nusselt number for the considered flow problem are

$$C_f = \frac{2\upsilon}{W_w}\left(\frac{\partial w}{\partial r}\right)_{r=a}, Nu = -\frac{ak}{(T_w - T_b)}\left(\frac{\partial T}{\partial r}\right)_{r=a}. \tag{21}$$

The nondimensional forms for the abovementioned physical properties are

$$\frac{z\mathrm{Re}}{a}(1-\phi)^{2.5}C_f = \frac{\partial^2 f(1)}{\partial \eta^2}, Nu = -2\frac{k_{nf}}{k_f}\frac{\partial \theta(1)}{\partial \eta}. \tag{22}$$

3. Solution by OHAM

The solution of the modeled problems in Equations (11) and (12), under the initial and boundary conditions of Equation (13) using the OHAM technique [8–10], have been utilized. The initial guesses have been calculated from the linear operators as follows:

$$\begin{array}{l} f_0(\eta) = \frac{3}{2}\left[\frac{\eta^3}{6} - \frac{\beta\eta^2}{2} + \left(\beta - \frac{1}{2}\right)\eta + \left(\frac{1}{3} - \frac{\beta}{2}\right)\right].\left[\frac{-2\beta A^*(1-\beta)^2}{(1-\beta)^3}\right] + \frac{A^*}{2}\left(\eta^2 + 1\right) + (1 - A^*)\eta, \\ \theta_0(\eta) = 1, \text{ such that } A^* = \frac{M}{\sqrt{\beta}}\theta(\beta)(1-\phi)^{2.5}. \end{array} \tag{23}$$

The initial guesses for the velocity and temperature profiles, which satisfy the physical conditions of Equations (12) and (13), have been calculated from the defined linear operators as

$$L_f = f^{iv}, L_\theta = \theta'', \tag{24}$$

The general solution of the linear operators is established as

$$L_f\left(C_1 + C_2\eta + C_3\eta^2 + C_4\eta^3\right) = 0 \quad and \quad L_\theta(C_5 + C_6\eta) = 0. \tag{25}$$

Here, $C_i (i = 1 - 6)$ are the constraints of the general solution.

The concept of the average squared residual errors applying the BVPh 2.0 package as defined by Liao [8] to find out the stable convergent solution of the problem has been used.

The Equations (10) and (11) with the physical conditions in Equations (12) and (13) of the proposed problems are defined as

$$\varepsilon_m^f = \frac{1}{n+1}\sum_{j=1}^{n}\left[\kappa_f\left(\sum_{j=1}^{n} f(\eta)_{\eta = j\delta\eta}\right)\right], \tag{26}$$

$$\varepsilon_m^{\theta} = \frac{1}{n+1}\sum_{j=1}^{n}\left[\kappa_{\theta}\left(\sum_{j=1}^{n} f(\eta)_{\eta=j\delta\eta}, \sum_{j=1}^{n} \theta(\eta)_{\eta=j\delta\eta}\right)\right], \tag{27}$$

The combined square residual error is shown as

$$\varepsilon_m^{t} = \varepsilon_m^{f} + \varepsilon_m^{\theta}. \tag{28}$$

The total square residual error up to the 20th-order approximations in the form of auxiliary parameters has been shown. The outputs of the optimal convergence controlling constraints $h_f = -0.5657$ and $h_{\Theta} = -1.3410$ have been achieved from the 20th-order OHAM approximation for the velocity and temperature profiles, respectively.

The average square residual error of the CNT nanofluid was calculated up to the 30th-order approximation for the SWCNT and MWCNT nanofluid and is shown in Tables 2 and 3, respectively. The increasing order of approximation reduces the residual error and strong convergence is achieved.

Table 2. The total sum of the averaged squared residual errors for the *SWCNTs*. When Pr = 6.7, M = Re = 0.1, $\phi = 0.01$.

m	ε_m^f *SWCNT*	ε_m^{Θ} *SWCNT*
6	1.36438×10^{-4}	2.86775×10^{-2}
12	7.14094×10^{-5}	1.48738×10^{-2}
18	5.20944×10^{-5}	1.07298×10^{-2}
24	4.37298×10^{-5}	8.54131×10^{-3}
30	3.95787×10^{-5}	7.94423×10^{-3}

Table 3. The total sum of the averaged squared residual errors for the *MWCNTs*. When Pr $= 6.7$, $M =$ Re $= 0.1$, $\phi = 0.01$

m	ε_m^f *MWCNT*	ε_m^{Θ} *SWCNT*
6	1.07991×10^{-4}	2.88574×10^{-2}
12	5.65266×10^{-5}	1.0759×10^{-2}
18	4.12383×10^{-5}	7.7877×10^{-3}
24	3.4616×10^{-5}	8.55721×10^{-3}
30	1.133×10^{-5}	8.00663×10^{-3}

4. Results and Discussion

In this article, the thin-film nanofluid spray comprised of SWCNT or MWCNT nanofluid under the Marangoni convection on the surface of an extending cylinder has been examined with regard to heat transfer enhancement applications. The Optimal Homotopy Analysis Method for Boundary Value Problem (OHAM-BVPh 2.0) package was used to obtain the solution of the problem. The error analysis was done to authenticate the obtained results. The physical and numerical outputs of the obtained results are displayed in figures and tables. Figure 1 shows the geometry of the problem. The total square residual error up to the 30th-order approximation for the SWCNTs and MWCNTs is displayed in Figures 2 and 3, respectively.

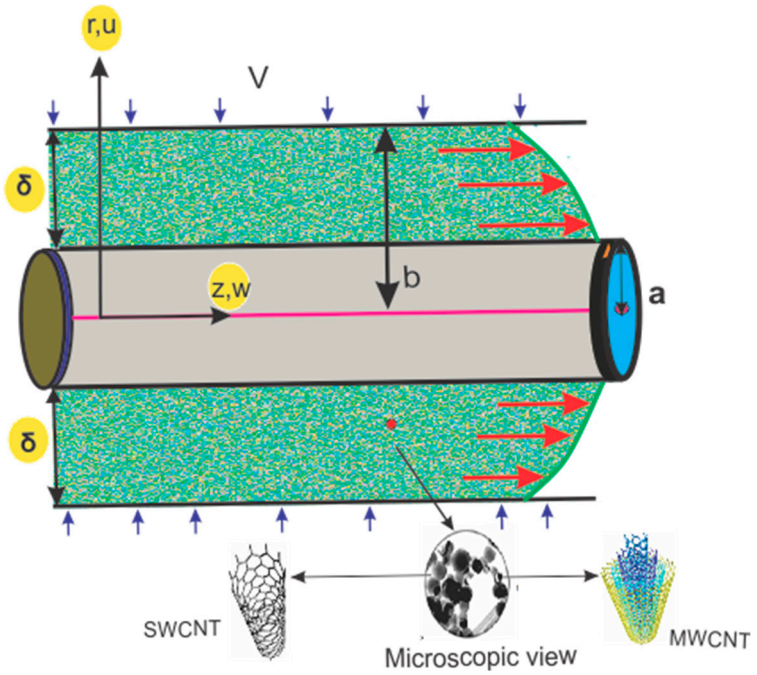

Figure 1. Geometry of the proposed problem for the thin film nanofluid flow.

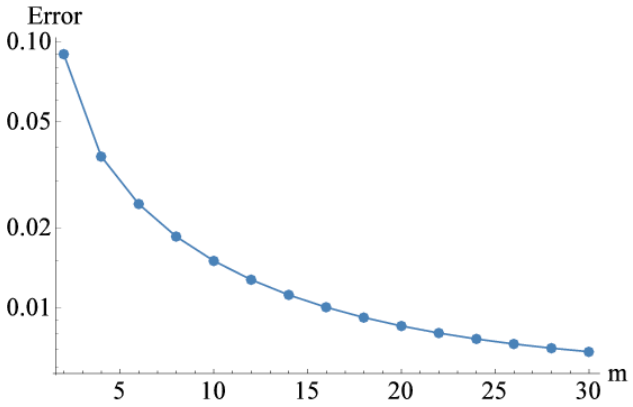

Figure 2. The total square residual error for the SWCNT nanofluid.

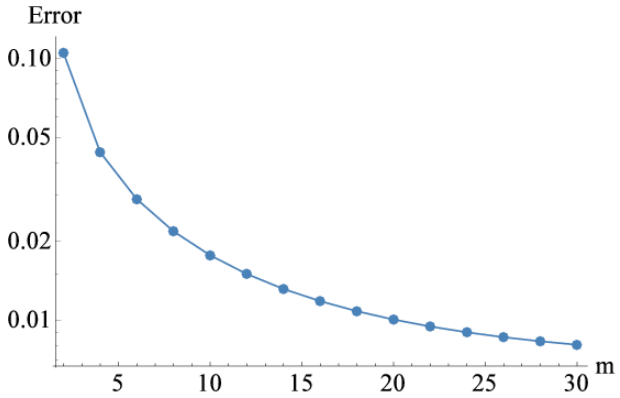

Figure 3. The total square residual error for the MWCNT nanofluid.

The impact of the parameters M, Re, ϕ, versus skin friction with SWCNTs and MWCNTs is displayed in Table 4. The larger values of the Marangoni convection parameter, M, enhances the skin friction and this effect is stronger in the SWCNTs, as shown in Table 4. The strong inertial forces stop the fluid motion and therefore the larger amount of Re enhances the skin friction. Further, this impact is

more dominant in the case of SWCNTs, as exhibited in Table 4. The increasing value of the nanoparticle volume fraction, ϕ, decreases the skin friction. In fact, larger values of ϕ enhance the thermal efficiency of the fluid to increase the velocity field and reduce the skin friction. The effect is more specific in the SWCNTs.

Table 4. The impact of M, Re, ϕ, versus skin friction. When Pr $= 6.7$, $\beta = 1.1$.

M	Re	$-f''(1)$, $\phi = 0.01$, SWCNTs	$-f''(1)$, $\phi = 0.02$, SWCNTs	$-f''(1)$, $\phi = 0.01$, MWCNTs	$-f''(1)$, $\phi = 0.02$, MWCNTs
0.1	0.01	5.7770	5.6035	2.07731	2.1142
0.95	0.01	5.788045	5.6060	0.85576	0.949745
	0.02	48.08882	46.5502	1.993255	2.0066227

The influence of the parameters Pr, Re, ϕ, versus the Nusselt number has been displayed in Table 5. Usually, the larger amount of the Prandtl number increases the Nusselt number. However, in the presence of strong Marangoni convection, this effect is more visible, as shown in Table 5. Also, this gap of influence is sufficiently large as compared to other published work. The rising values of Re, ϕ, decrease the Nusselt number, and again, the effect is comparatively strong for the small change in the values of these parameters. Further, this impact is stronger in the case of SWCNTs. The comparison of the OHAM and numerical method has been displayed in Table 6. This shows that the obtained results are in close agreement.

Table 5. The impact of Pr, Re, ϕ, versus the Nusselt number. When $\beta = 1.1$, $M = 1.7$.

Pr	Re	$-\theta'(1)$, $\phi = 0.01$, SWCNTs	$-\theta'(1)$, $\phi = 0.02$, SWCNTs	$-\theta'(1)$, $\phi = 0.01$, MWCNTs	$-\theta'(1)$, $\phi = 0.02$, MWCNTs
5	0.02	34.6345	9.520555	29.8314	8.62064
5.5		38.96033	10.7574	33.1675	9.74325
	0.02	99.5200	66.01308	88.9056	88.6201
	0.03	57.8527	55.955591	49.9839	48.3375

The inertial forces enhance with the increasing value of the Reynolds number, and consequently, the velocity field decreases, as shown in the Figure 4. Due to the Marangoni convection, this effect is limited and the velocity field starts to increase after the critical point. This point varies with the variation of the physical parameters and plays an important role during the thin film spray. Further, this impact is relatively stronger in the SWCNTs.

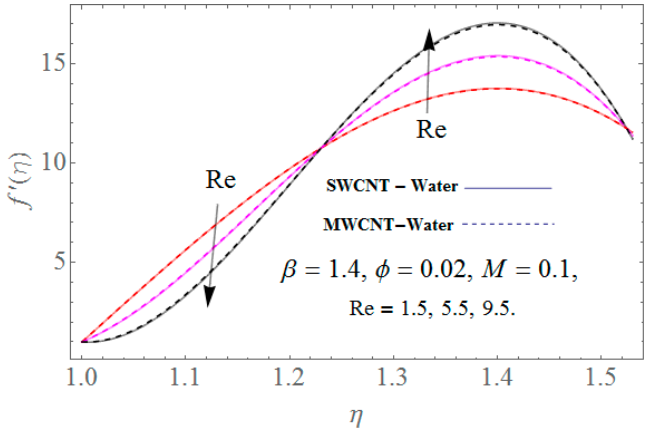

Figure 4. The impact of the Reynolds number versus the velocity field.

The SWCNTs and MWCNTs are clearly visible during the increasing values of the Marangoni convection, as shown in Figure 5. The increasing value of the Marangoni convection parameter reduces

the velocity field. The increasing convection enhances the resistance force to reduce the fluid motion. This effect is very closed for both types of CNTs. After the point where $\eta = 1.7$, the resistance force reduces and the effect of the Marangoni convection is diverted towards the free surface.

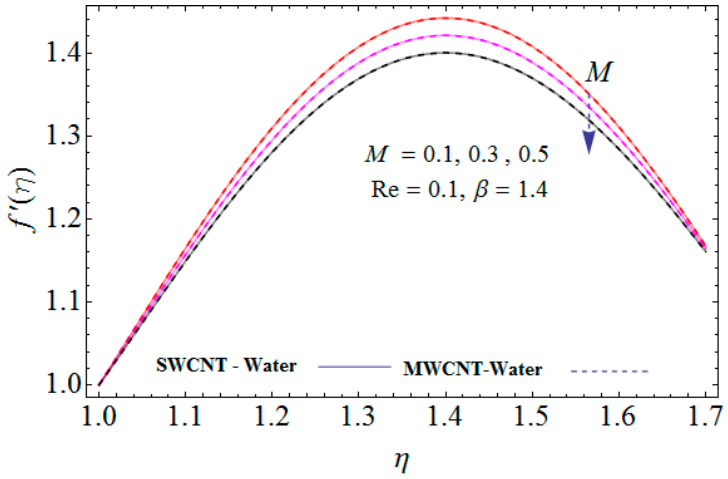

Figure 5. The impact of the Marangoni convection parameter versus the velocity field.

The increasing value of the thin film thickness parameter β decreases the fluid motion, as shown in Figure 6. Physically, the resistive force enhances with the increasing value of β, and consequently, the velocity profile decreases. The increasing values of the nanoparticle volume fraction cause the radial velocity to rise near the cylinder surface and the velocity field is retarded after the point of inflection, as displayed in Figure 7. The Marangoni convection changes the effect of the nanoparticle volume fraction, and this effect is comparatively stronger in the SWCNTs. It has been observed that the point of inflection varies with the variation in the Marangoni convection parameter values and plays an important role in the limitation of the thin film spray.

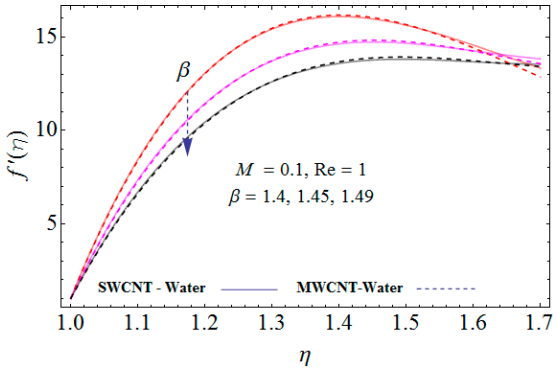

Figure 6. The impact of the thin film thickness parameter versus velocity field.

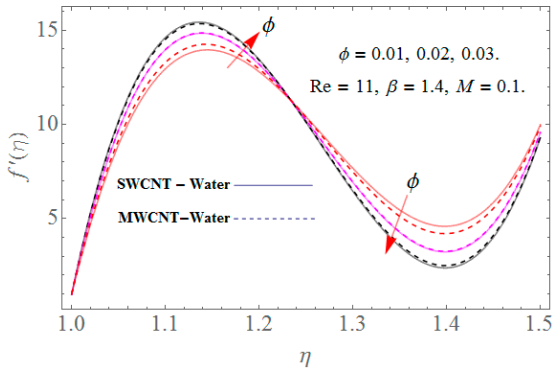

Figure 7. The impact of the nanoparticle volume fraction versus the velocity field.

Figure 8 shows that increase in the Prandtl number decreases the temperature profile. In fact, the thickness of the momentum boundary layer becomes larger than the thermal boundary layer, i.e., the viscous diffusion is larger than the thermal diffusion, and therefore, the larger value of the Prandtl number reduces the thermal boundary layer. Figure 9 displays the effect of the increasing value of the thin film thickness parameter β versus temperature field. The larger amount of the parameter β increases the cooling effect and the temperature field decreases. This decreasing effect is very similar for both types of nanofluids.

The increasing values of the Reynolds number enhance the inertial forces to generate the resistance force, which decreases the pressure distribution near the cylinder surface, as shown in Figure 10. Due to the Marangoni convection, the pressure distribution is enhanced in the middle after the critical point, and this variation is continued through the whole thin film spray process. Clearly, this effect is stronger using the SWCNTs as compared to the MWCNTs. The pressure distribution decreases with increasing values of the Prandtl number near the cylinder surface, as depicted in Figure 11. Due to the existence of the Marangoni convection, the pressure distribution increases after the point of inflection, and this variation is continued in the SWCNTs and MWCNTs. The increasing values of the nanoparticle volume fraction increase the viscosity of the fluid and the pressure distribution decreases near the wall surface, as shown in Figure 12. This effect varies in the presence of Marangoni convection after the point of inflection. The variation in the effect of the two types of CNTs is more visible due to the intermolecular forces and wide range of pressure distribution. The increasing value of the thin film thickness generates the resistance force and the pressure distribution decreases near the wall surface, as displayed in Figure 13. The Marangoni convection stops this decrease and pressure distribution starts to increase after the critical point. The increasing and decreasing effect also varies in both SWCNTs and MWCNTs.

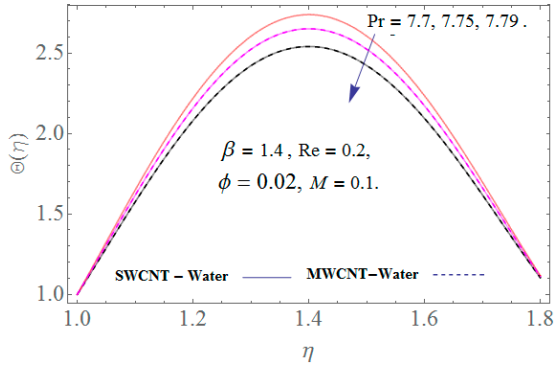

Figure 8. Impact of the Prandtl number versus temperature field.

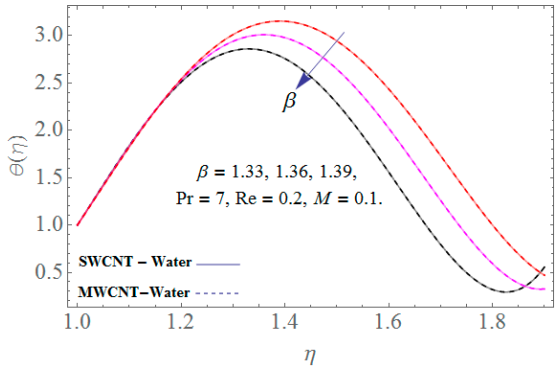

Figure 9. The impact of the thin film thickness parameter versus temperature field.

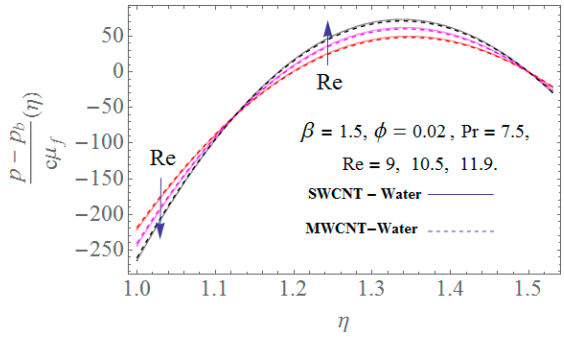

Figure 10. Impact of the Reynold number versus pressure distribution.

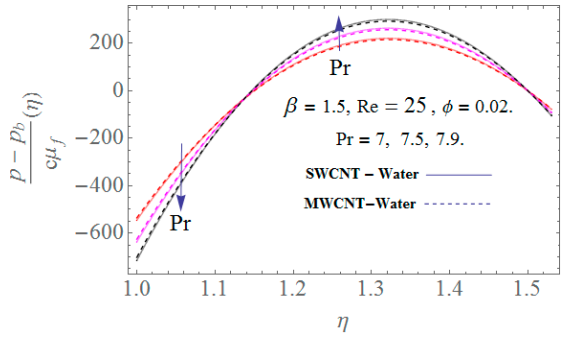

Figure 11. The impact of the Prandtl number versus the velocity field.

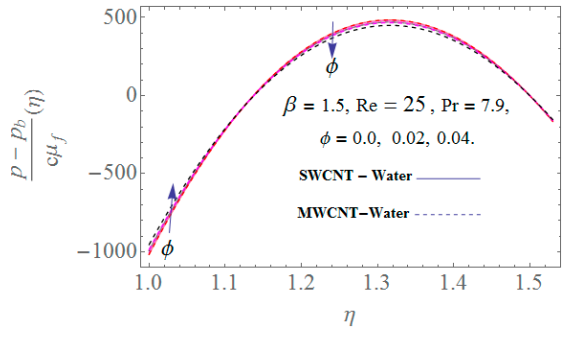

Figure 12. Impact of the nanoparticle volume fraction versus pressure distribution.

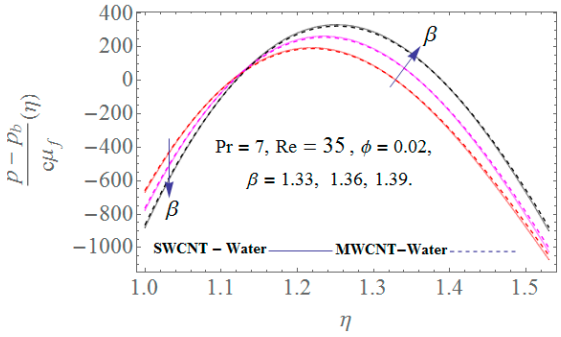

Figure 13. Impact of the thickness parameter versus pressure distribution.

Table 6. OHAM and numerical comparison for $f(\eta)$. When $\mathrm{Pr} = 7.7, \beta = 1.5, \mathrm{Re} = 1.4,\ \phi = 0.01$.

η	OHAM	Numerical	Absolute Error
1	1.000000	1.000000	9.037220×10^{-14}
1.2	1.088720	1.088720	2.276710×10^{-8}
1.4	0.997348	0.997348	1.734450×10^{-8}
1.6	0.768098	0.768098	1.702170×10^{-8}
1.8	0.428282	0.428282	2.176850×10^{-8}
2	1.979060	1.979060	2.388290×10^{-8}

5. Conclusions

The thin film spray of water-based CNT nanofluids over the surface of an extending cylinder for thermal applications has been examined in this research. The two types of carbon nanotubes, known as SWCNTs/MWCNTs, have been used for the spray pattern under the Marangoni convection. The solution of the modeled nonlinear differential equations has been obtained through OHAM. The total square residual error has been calculated for the velocity and temperature profiles, respectively. The obtained outputs are shown as follows. It is observed that the increasing thickness of the thin film β reduces the spray rate near the wall surface, and this effect changes after the critical point due to the Marangoni convection. This effect is more efficient in the case of the SWCNTs as compared to the MWCNTs. It is observed that with larger values of the nanofluid volume fraction ϕ, the thin film flow increases near the cylinder surface and varies inversely after the point of inflection. The variation in the effect of ϕ is due to the existence of Marangoni convection. The SWCNT nanofluid is more affected as compared to the MWCNT nanofluid. It has been observed that the impact of the parameters varies with the variation of the Marangoni convection, and one can move the point of inflection during the thin film spray for uniformity. Also, based on most of the obtained results, the effect of variation is stronger in the SWCNTs.

Future work: This findings of this study are extendable to:

(1) Slip boundary conditions;
(2) Heat and mass transfer;
(3) Entropy generation;
(4) Porous space and Hall effects;
(5) Cu–water nanofluids and so on.

Author Contributions: Conceptualization: A.R. and T.G.; methodology: Z.S. and S.M.; software: P.K.; validation: T.G. and A.R.; formal analysis: F.H.; investigation: P.K.; writing—original draft preparation: T.G. and A.R.; writing—review and editing: T.G., Z.S., S.M., F.H., K.S.N., and P.K.

Funding: This research was funded by the Center of Excellence in Theoretical and Computational Science (TaCS-CoE), KMUTT.

Acknowledgments: This project was supported by the Theoretical and Computational Science (TaCS) Center under Computational and Applied Science for Smart Innovation Research Cluster (CLASSIC), Faculty of Science, KMUTT.

Conflicts of Interest: The authors declare that they have no conflict of interest.

Nomenclature

ϕ	solid particle volume fraction	a	radius of the cylinder
ρ_{nf}	density of the nanofluid	μ_{nf}	dynamic viscosity of nanofluid
k_f	thermal conductivity of the base fluid	k_{nf}	thermal conductivity of the nanofluid
k_{CNT}	thermal conductivities of the nanosolid particles	T	temperature profile (K)
$(\rho C_p)_{nf}$	specific heat capacity of the nanofluid	$\sigma^{\otimes}$	surface tension
C_f	skin friction	ρ_f	density of the base fluid (kg/m^3)
T_b	ambient temperature (K)	σ	surface tension at origin
T_{ref}	reference temperature (K)	$c > 0$	stretching constant
u	velocity in the r-direction (m/s)	U_w	surface velocity (m/s)
T_w	surface temperature (K)	Pr	Prandtl number
$(\rho c_p)_f$	specific heat capacity of the base fluid	w	velocity in the z-direction (m/s)
η	similarity variable	μ_f	dynamic viscosity of the base fluid
b	outer radius	r	radial direction (m)
p	pressure	z	axis of the cylinder (m)
$c < 0$	shrinking constant	W_w	stretching velocity (m/s)

References

1. Chen, C.H. Marangoni effects on forced convection of power-law liquids in a thin film over a stretching surface. *Phys. Lett. A* **2007**, *370*, 51–57. [CrossRef]
2. Liu, F.; Darjani, S.; Akhmetkhanova, N.; Maldarelli, C.; Banerjee, S.; Pauchard, V. Mixture effect on the dilatation rheology of asphaltenes-laden interfaces. *Langmuir* **2017**, *33*, 1927–1942. [CrossRef] [PubMed]
3. Mozaffri, A.; Mood, N.S.; Koplik, J.; Maldarelli, C. Self-diffsiophoretic colloidal propulsion near a solid boundary. *Phys. Fluids* **2016**, *28*, 053107. [CrossRef]
4. Mozaffari, S.; Tchoukov, P.; Atias, J.; Nazemifard, N. Effect of Asphaltene Aggregation on Rheological Properties of Diluted Athabasca Bitumen. *Energy Fuels* **2015**, *29*, 5595–5599. [CrossRef]
5. Mozaffari, S.; Tchoukov, P.; Mozaffari, A.; Atias, J.; Czarnecki, J.; Nazemifard, N. Capillary Driven Flow in Nanochannels—Application to Heavy Oil Rheology Studies. *Colloids Surf. A Physicochem. Eng. Asp.* **2017**, *513*, 178–187. [CrossRef]
6. Kumar, K.G.; Gireesha, B.J.; Krishnamurthy, M.R.; Prasannakumara, B.C. Impact of convective condition on Marangoni convection flow and heat transfer in Casson nanofluid with uniform heat source sink. *J. Nanofluids* **2018**, *7*, 108–114. [CrossRef]
7. Haq, R.U.; Kazmi, S.N.; Mekkaoui, T. Thermal management of water based SWCNTs enclosed in a partially heated trapezoidal cavity via FEM. *Int. J. Heat Mass Transf.* **2017**, *112*, 972–982. [CrossRef]
8. Iijima, S. Helical microtubules of graphitic carbon. *Nature* **1991**, *354*, 56–58. [CrossRef]
9. Ajayan, P.M.; Iijima, S. Capillarity-induced filling of carbon nanotubes. *Nature* **1993**, *361*, 333–334. [CrossRef]
10. To, C.W.S. Bending and shear moduli of single–walled carbon nanotubes. *Finite Elem. Anal. Des.* **2006**, *42*, 404–413. [CrossRef]
11. Dresselhaus, M.S.; Dresselhaus, G.; Saito, R. Physics of carbon nanotubes. *Carbon* **1995**, *33*, 883–891. [CrossRef]
12. Hone, J. Carbon nanotubes: Thermal properties. *Dekker Encycl. Nanosci. Nanotechnol.* **2004**, *7*, 603–610.
13. Haq, R.U.; Nadeem, S.; Khan, Z.H.; Noor, N.F.M. Convective heat transfer in MHD slip flow over a stretching surface in the presence of carbon nanotubes. *Phys. B Condens. Matter* **2015**, *457*, 40–47. [CrossRef]
14. Khan, W.A.; Khan, Z.H.; Rahi, M. Fluid flow and heat transfer of carbon nanotubes along a flat plate with Navier slip boundary. *Appl. Nanosci.* **2014**, *4*, 633–641. [CrossRef]
15. Kamali, R.; Binesh, A.R. Numerical investigation of heat transfer enhancement using carbon nanotube-based non-Newtonian nanofluids. *Int. Commun. Heat Mass Transf.* **2010**, *37*, 1153–1157. [CrossRef]
16. Liu, M.S.; Lin, M.C.C.; Te, H.I.; Wang, C.C. Enhancement of thermal conductivity with carbon nanotube for nanofluids. *Int. Commun. Heat Mass Transf.* **2005**, *32*, 1202–1210. [CrossRef]
17. Halelfadi, S.; Mare, T.; Estelle, P. Efficiency of carbon nanotubes water based nanofluids as coolants. *Exp. Therm. Fluid Sci.* **2014**, *53*, 104–110. [CrossRef]

18. Lebon, G.; Machrafi, H. Thermal conductivity of tubular nanowire composites based on a thermodynamical model. *Physica E* **2015**, *71*, 117–122. [CrossRef]
19. Machrafi, H.; Lebon, G. Thermal Conductivity of Spherical P articulate Nanocomposites: Comparison with Theoretic al Models, Monte Carlo Simulations and Experiments. *Int. J. Nanosci.* **2014**, *13*, 1450022. [CrossRef]
20. Lebon, G.; Machrafi, H. A thermodynamic model of nanofluid viscosity based on a generalized Maxwell type constitutive equation. *J. Non-Newton. Fluid Mech.* **2018**, *253*, 1–6. [CrossRef]
21. Xue, Q. Model for thermal conductivity of carbon nanotube-based composites. *Phys. B Condens. Matter* **2005**, *368*, 302–307. [CrossRef]
22. Aman, S.; Khan, I.; Ismail, Z.; Salleh, M.Z.; Al-Mdallal, Q.M. Heat transfer enhancement in free convection flow of CNTs Maxwell nanofluids with four different types of molecular liquids. *Sci. Rep.* **2017**, *7*, 2445. [CrossRef]
23. Gul, T.; Khan, W.A.; Tahir, M.; Bilal, R.; Khan, I.; Nisar, K.S. Unsteady Nano-Liquid Spray with Thermal Radiation Comprising CNTs. *Processes* **2019**, *7*, 181. [CrossRef]
24. Zhang, J.; Liu, X. Dispersion Performance of Carbon Nanotubes on Ultra-Light Foamed Concrete. *Processes* **2018**, *6*, 194. [CrossRef]
25. Wang, C.Y. Liquid film on an unsteady stretching surface. *Q. Appl. Math.* **1990**, *48*, 601–610. [CrossRef]
26. Andersson, H.I.; Aarseth, J.B.; Dandapat, B.S. Heat transfer in a liquid film on an unsteady stretching surface. *Int. J. Heat Mass Transf.* **2000**, *43*, 69–74. [CrossRef]
27. Chen, C.H. Heat transfer in a power-law fluid film over a unsteady stretching sheet. *Heat Mass Transf.* **2003**, *39*, 791–796. [CrossRef]
28. Chen, C.H. Effect of viscous dissipation on heat transfer in a non-Newtonian liquid film over an unsteady stretching sheet. *J. Non-Newton. Fluid Mech.* **2006**, *135*, 128–135. [CrossRef]
29. Wang, C. Analytic solutions for a liquid film on an unsteady stretching surface. *Heat Mass Transf.* **2006**, *42*, 759–766. [CrossRef]
30. Dandapat, B.S.; Santra, B.; Andersson, H.I. Thermocapillarity in a liquid film on an unsteady stretching surface. *Int. J. Heat Mass Transf.* **2003**, *46*, 3009–3015. [CrossRef]
31. Liu, I.C.; Wang, H.H.; Peng, Y.F. Flow and heat transfer for three dimensional flow over an exponentially stretching surface. *Chem. Eng. Commun.* **2012**, *200*, 253–268. [CrossRef]
32. Khan, Y.; Wu, Q.; Faraz, N.; Yildirim, A. The effects of variable viscosity and thermal conductivity on a thin film flow over a shrinking/stretching sheet. *Comput. Math. Appl.* **2011**, *61*, 3391–3399. [CrossRef]
33. Abel, M.S.; Mahesha, N.; Tawade, J. Heat transfer in a liquid film over an unsteady stretching surface with viscous dissipation in presence of external magnetic field. *Appl. Math. Model.* **2009**, *33*, 3430–3441. [CrossRef]
34. Narayana, M.; Sibanda, P. Laminar flow of a nanoliquid film over an unsteady stretching sheet. *Int. J. Heat Mass. Transf.* **2012**, *55*, 7552–7560. [CrossRef]
35. Wang, C.Y. Liquid film sprayed on a stretching surface. *Chem. Eng. Commun.* **2006**, *93*, 869–878. [CrossRef]
36. Khan, N.S.; Gul, T.; Islam, S.; Khan, I.; Alqahtani, A.M.; Alshomrani, A.S. Magnetohydrodynamic nanoliquid thin film sprayed on a stretching cylinder with heat transfer. *Appl. Sci.* **2017**, *7*, 271. [CrossRef]
37. Alshomrani, A.S.; Gul, T. A convective study of Al_2O_3-H_2O and Cu-H_2O nano-liquid films sprayed over a stretching cylinder with viscous dissipation. *Eur. Phys. J. Plus* **2017**, *132*, 495–511. [CrossRef]
38. Gul, T.; Nasir, S.; Islam, S.; Shah, Z.; Khan, M.A. Effective Prandtl Number Model Influences on the γAl_2O_3–AH_2O and γAl_2O_3–$C_2H_6O_2$ Nanofluids Spray Along a Stretching Cylinder. *Arab. J. Sci. Eng.* **2018**, *44*, 1601–1616. [CrossRef]
39. Liao, S.J. An optimal homotopy-analysis approach for strongly nonlinear differential equations. *Commun. Nonlinear Sci. Numer. Simul.* **2010**, *15*, 2003–2016. [CrossRef]
40. Gul, T.; Firdous, K. The experimental study to examine the stable dispersion of the graphene nanoparticles and to look at the GO–H_2O nanofluid flow between two rotating disks. *Appl. Nanosci.* **2018**, *8*, 1711–1727. [CrossRef]
41. Gul, T.; Haleem, I.; Ullah, I.; Khan, M.A.; Bonyah, E.; Khan, I.; Shuaib, M. The study of the entropy generation in a thin film flow with variable fluid properties past over a stretching sheet. *Adv. Mech. Eng.* **2018**, *10*, 1–15. [CrossRef]
42. Taza, G.; Waris, K.; Muhammad, S.; Muhammad, A.K.; Ebenezer, B. MWCNTs/SWCNTs Nanofluid Thin Film Flow over a Nonlinear Extending Disc: OHAM Solution. *J. Therm. Sci.* **2019**, *28*, 115–122. [CrossRef]